Wideband Measurement-Based Modeling of Inter-Vehicle Channels in the 5 GHz Band

Olivier Renaudin, Veli-Matti Kolmonen, Pertti Vainikainen, and Claude Oestges

***Abstract*—In this paper, we describe a new wideband Single-Input Single-Output (SISO) channel model for Vehicle-to-Vehicle (V2V) channels, based on an extensive measurement campaign that has been carried out at 5.2 GHz around Helsinki (Finland) in August 2007. Both the now well-known non-stationary behavior and the measured characteristics of the V2V channel motivate the use of a Geometry-based Stochastic Channel Modeling (GSCM) approach rather than a classical tapped-delay line one. For the time-variant contributions stemming from discrete scatterers, the propagation distance can be estimated deterministically (i.e. geometrically), whereas the fading can be modeled as the combination of a distance-decaying process and two stochastic small- and large-scale processes. The complete parameterization of the V2V wideband channel model, the recipe for its implementation and the analysis of its validity are also provided in the paper.**

***Index Terms*—Channel sounding, vehicular radio propagation channels, geometry-based stochastic modeling.**

I. Introduction

In the last few years, Intelligent Transportation System (ITS) infrastructures based on mobile-to-mobile wireless communications have received a lot of attention. Various kinds of new applications are expected for V2V communications, ranging from road traffic safety (e.g. collision avoidance, congestion prediction, etc.) to social networking and multimedia services. In V2V communication systems, vehicles would be considered as nodes in a mobile ad-hoc network, which implies that cellular wireless networks (with fixed base stations) are not required for communications between vehicles.

The IEEE 802.11p standard [1], also known as Wireless Access in Vehicular Environments (WAVE), will enable V2V communications in the 5 GHz band and denotes the growing interest in this area. The design and deployment of the IEEE 802.11p, as well as alternative V2V wireless communication systems, requires the knowledge of the underlying V2V radio propagation channel characteristics, which differ significantly from those of classical cellular wireless networks because (i): both the transmitter (Tx) and the receiver (Rx) are mobile, (ii): the antennas have relatively low heights and (iii): the scattering environment can change very rapidly.

There is therefore a strong requirement of knowledge about the properties of V2V radio propagation channels. To do so, Single-Input Single-Output (SISO) or Multiple-Input Multiple-Output (MIMO) V2V channels have to be investigated in order to derive accurate models, able to reliably reproduce the time-variant behavior of their characteristics. Different approaches can be considered for that purpose, i.e. (i): deterministic, (ii): stochastic or (iii): geometry-based stochastic [2], [3].

Deterministic methods consist in (approximated) solutions of Maxwell's equations. They require an accurate modeling of the physical objects in the environment to be simulated (e.g. the surrounding buildings, vegetation, traffic signs, vehicles, etc.), including their respective shapes, locations and scattering properties [4], [5]. However, even if they are very realistic and accurate, these approaches are computationally intensive. They are therefore used only for specific applications (e.g. for antenna placement [6], etc.), as they appear to be not well suited for high-level simulation systems.

Stochastic approaches consist in the modeling of the channel according to some of its parameters, e.g. Root-Mean-Square (RMS) delay and Doppler spreads, Doppler spectra, angles of departure/arrival, etc. Tapped-Delay Line (TDLs) are probably the most popular stochastic channel models, where each tap is assumed to fade independtly with given channel statistics, based on the Wide-Sense Stationary Uncorrelated Scattering (WSSUS) assumption. Their low complexity and easy implementation make them very attractive in high-level simulation systems such as the IEEE 802.11p standard. Different V2V TDL models at 2.4 GHz are also given in [7], [8], including Doppler spectra for each tap. Though, as V2V channels are now widely known to exhibit a non-stationary behavior [9], [10], i.e. fast time-varying statistics, the WSSUS assumption can remain valid only over short time intervals: TDL models are hence not able to reproduce realistic properties of the V2V channels. Various solutions have been proposed in the literature in order to overcome this limitation, by means of (i): "birth/death" Markov processes to model the appearance and disappearance of taps [11], (ii): different TDL models depending on the delay spread and the Bit Error Rate (BER) statistics [8] or also (iii): time-variant statistics estimated over time intervals where the channel is stationary [12]. All these methods can however not model strong discrete scatterer contributions drifting from one tap to another.

The Geometry-based Stochastic Channel Modeling (GSCM) approach is a combination of the two previous deterministic and stochastic approaches. The radio wave propagation and the scattering aspects are indeed decoupled, with (i): scatterers placed in the environment around both the Tx and Rx vehicles either at random, e.g. according to two-ring [13], two-cylinder [14] or also two-ring elliptical [15] models, or

O. Renaudin and C. Oestges are with the Université catholique de Louvain (UCL), ICTEAM Electrical Engineering, 1348 Louvain-la-Neuve, Belgium (e-mails: olivier.renaudin@uclouvain.be, claude.oestges@uclouvain.be).

V.M. Kolmonen is with Philips Medical Systems MR Finland. P. Vainikainen was with the Aalto University SMARAD Radio Science and Engineering, FI-02015 TKK, Finland.

at physically realistic positions, such that their contributions can be determined using very simplified ray-tracing methods (e.g. assuming only single or double reflections, etc.), (ii): fading properties assigned to each scatterer [16], [17]. The total wideband channel corresponds to the sum at the receiver side of all these scatterer contributions. This approach was found to inherently model the non-stationary behavior of the channel, since it includes the dynamic nature of the scattering environment geometry.

In this paper, we present such a GSCM of V2V channels, based on a measurement campaign conducted in various environments around Helsinki (Finland). Although the framework of this model is similar to the one proposed in [17] for the extraction and the modeling of the Line-of-Sight (LoS) component and the discrete scatterer contributions, our modeling approach differs, sometimes significantly, as

- We model and completely parameterize the fading for the LoS component and discrete scatterer contributions in a purely stochastic manner,
- We model and completely parameterize the diffuse scattering in a purely stochastic manner, based on the approach proposed in [18]. This approach differs indeed from the one in [17], where "walls" of diffuse scatterers located along the road were considered.

The V2V channel model proposed in this paper aims also at validating the one presented in [17], though it is validated only for SISO systems (as the patterns of the measurement antennas were not known exactly). However, note that it can be easily generalized to MIMO systems, by considering an appropriate antenna pattern.

This paper will be organized as follows: Section II describes the measurement campaign. Section III presents the general outline of the V2V channel model, with a detailed description of the discrete and diffuse scattering and their parameterization from the measured Channel Impulse Responses (CIRs). Section IV proposes the step-by-step implementation recipe as well as the validation of the V2V channel model. Finally, Section V provides a conclusion.

II. V2V Measurement Campaign

In this Section, we describe the measurement campaign that is used for the parameterization of the model. More details about this measurement campaign can be found in [9].

A. Experimental Set-Up

The V2V channel measurement campaign was carried out using the channel sounder of Aalto University, which performs MIMO measurements at 5.3 GHz with 60 MHz bandwidth [19]. The maximum transmit power was 36 dBm (i.e. 3.98 W). The snapshot time was set at $t_{\text{snap}} = 8.4$ ms, while the macroscopic snapshot repetition rate ν_{rep} was set at 14.3 Hz to limit the recorded file sizes. Hence, the maximum resolvable Doppler shift ν_{max} is limited to 7.15 Hz, which corresponds to a maximum relative speed of 0.41 m/s. The main channel sounder parameters are summarized in Table I.

TABLE I
Channel Sounder Parameters

Center frequency, f	5.3 GHz
Measurement bandwidth, BW	60 MHz
Sampling frequency, F_{s}	120 MHz
Delay resolution, $\Delta\tau = 1/BW$	16.7 ns
Transmit power, P_{Tx}	36 dBm
Snapshot time, t_{snap}	8.4 ms
Snapshot repetition rate, $\nu_{\text{rep}} = 1/t_{\text{rep}}$	14.3 Hz
Maximum resolvable Doppler shift, ν_{max}	7.15 Hz

B. Antenna Arrays

The Tx and Rx antenna arrays were mounted on a wooden platform on the car roofs and covered with a plastic tarpaulin so as to protect them from air streams and rain. They consisted in semispherical antenna arrays with 16 dual-polarized elements (i.e. 32 feeds) arranged in a spherical geometry [19]. Polarizations were horizontal and vertical in the Rx antenna array, while the elements were slanted 45 degrees in the Tx antenna array. A discone antenna was used at both the Tx and Rx sides for adjusting the Automatic Gain Control (AGC) of the channel sounder. The 15 remaining antenna elements at both the Tx and Rx were thus selected in order to form the MIMO channel matrix, leading to $N_{\text{r}} \times N_{\text{t}} = 30 \times 30$ temporal multiplexed channels.

C. Vehicles and Routes

The Tx and Rx vehicles were traveling in the same direction, the Tx vehicle in front of the Rx vehicle. Note that other scenarios (e.g. with Tx and Rx vehicles traveling in opposite directions) were not considered. The measurement campaign was conducted in four different environments: on a campus (Otaniemi), on a highway (Ring 1), in urban (Helsinki) and sub-urban (Matinkyl, Leppvaara) areas,

- The campus and sub-urban areas are very similar and consist in small detached houses, parking lots and an average tree density. There are large sidewalks and road signs sparsely distributed on both sides of the two-lane road as well as little to no traffic conditions,
- The six-lane highway is located in a sub-urban like area. The roadsides consist in natural (or artificial) embankments and low-height buildings, excepted around the exit ramps. There is a median strip with some vegetation and delimited by guardrails, while there are some roadsigns scattered along the road. The Tx and Rx vehicles were driven on the hard shoulder, while traffic conditions ranged from light to medium,
- The urban area is the city center of Helsinki, with six to eight-storey buildings on both sides of the two-lane streets, medium to heavy traffic conditions and numerous roadsigns. Occasional blockage of the LOS occurred due to large vehicles (e.g. buses, trucks, etc.) or buildings when the Tx vehicle turned a corner.

The vehicles' speed was in the range of 5 - 15 km/h, so that the channel coherence is, in the worst case, still larger than

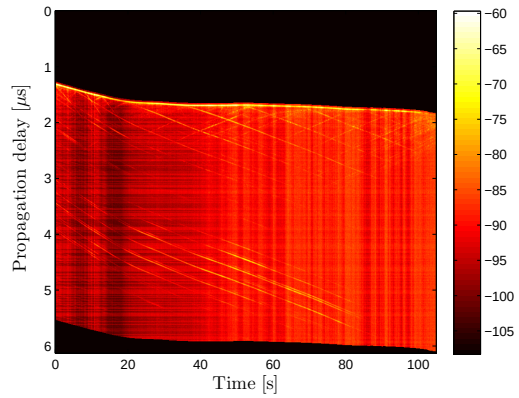

Fig. 1. Time-variant average Power-Delay Profiles (PDPs) measured in the highway environment.

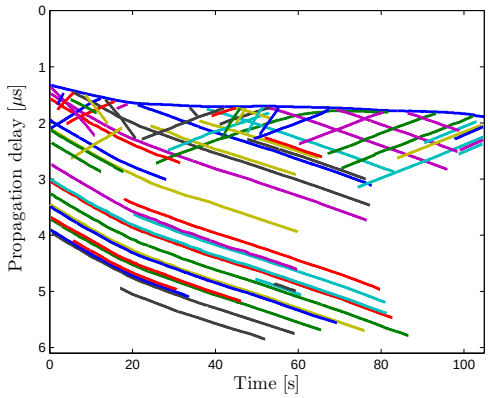

Fig. 2. Time-variant discrete scatterer contributions, extracted from the PDPs measured in the highway environment shown in Fig. 1.

t_{snap}. The inter-vehicle distance varied between 10 and 500 m, depending on the traffic conditions and the environment.

D. Measured Data

At the output of the channel sounder, we obtain the complex wideband $N_{\text{r}} \times N_{\text{t}} = 30 \times 30$ MIMO channel matrices

$$\mathbf{H}(\tau, t, q), \tag{1}$$

where τ, t and q correspond to the delay, time and antenna pair, respectively. In the following, we will concentrate on a single antenna sub-link $h(\tau, t)$ (out of $N_r \times N_t$), such that its Tx and Rx antenna elements are facing one another.

Note that the RF cable losses were normalized from the measured data after a back-to-back calibration procedure done before the measurement campaign. On the other hand, the Tx and Rx antenna gains were not de-embedded from the measured data (as the patterns of the antennas used during the measurement campaign were not known exactly) and are therefore taken into account in the further analysis.

III. Description of the Channel Model

In this Section, we provide the general outline of the V2V SISO channel model as well as the detailed description and parameterization of its different parts.

A. General Outline of the Channel Model

As shown in Fig. 1, the time-variant IRs can be divided into three different parts, i.e. (i): the LoS component, (ii): discrete contributions stemming off from either static or mobile scatterers that can drift strongly in the delay domain and (iii): diffuse scattering, which corresponds to numerous low-power contributions resulting from multiple-scattering or diffraction processes that can not be associated with discrete scatterers. Based on these observations, the time-variant IRs can then be expressed as follows [17]

$$h(\tau, t) = h_{\text{LOS}}(\tau_{\text{LOS}}, t) + \sum_{p=1}^{P} h_p(\tau_p, t) + h_{\text{d}}(\tau, t), \tag{2}$$

where P is the number of contributions stemming off from discrete either static or mobile scatterers. More specifically, the p^{th} discrete scatterer contribution can be modeled as [17]

$$\begin{aligned} h_p(\tau_p, t) = a_p(d_p) e^{j2\pi\nu_p t} \\ \times \delta(\tau - \tau_p)\delta(\Omega - \Omega_{\text{Tx},p})\delta(\Omega - \Omega_{\text{Rx},p}), \end{aligned} \tag{3}$$

where $d_p = c \cdot \tau_p$ (with c the speed of light), ν_p, $\Omega_{\text{Tx},p}$ and $\Omega_{\text{Rx},p}$ are the time-variant propagation distance, Doppler shift, angles of departure and arrival of the p^{th} discrete scatterer contribution, respectively. Its complex amplitude $a_p(d_p)$ includes the effects of the Tx and Rx antenna patterns, which is fading as it may include several unresolvable paths (owing to the limited measurement bandwidth of the system). The LoS component can be modeled similarly, by replacing the sub-index p by LoS in (3).

B. Extraction Procedure

The LoS component and the discrete scatterer contributions were identified from the Power-Delay Profiles (PDPs) given by $|h(\tau_k, t)|^2$. To do so, we used a search-and-subtract procedure whose different steps can be summarized as follows:

- Select a number of multipath components that are likely to belong to the same discrete scatterer contribution. They have to be sampled roughly every second and such that it includes the component with the strongest power,
- Interpolate the so selected multipath components in order to determine the underlying discrete scatterer contribution. Store the time-variant delay and amplitude of this contribution into vectors,
- Filter out this contribution from the measured PDPs, so that no artifact contribution (with much weaker power, surrounding the "true" one) can later be extracted,
- Iterate until no additional discrete scatterer contribution with an average power at least 6 dB above the noise level can be identified.

All the discrete scatterer contributions are assumed to have been captured by the extraction procedure, so that the remaining "cleaned" IRs consist in diffuse scattering and noise. Fig.

TABLE II
PARAMETERS OF THE RADIO WAVE PROPAGATION ASPECTS

	Parameters	Unit	Campus	Urban	Sub-Urban	Highway
Road parameters	N_{lanes}	-	4	2	4	7
	W_{lane}	[m]	2.75			
Scatterer densities	$\chi_{p,s}$	[m^{-1}]	0.12	0.13	0.12	0.10
	$\chi_{p,m}$	[m^{-1}]	0.03	0.05	0.03	0.08
Scatterer "birth/death"	$\mu_{b/d}$	[m]	4.80			5.26
	$\xi_{b/d}$	[m]	0.78			0.99
Static discrete scatterers	$\mu_{d,l=1}$	[m]	$\pm(N_{\text{lanes}}/2+1)W_{\text{lane}}$			
	$\mu_{d,l=2}$	[m]				
	$\mu_{d,l=3}$	[m]	-	-	-	0
	ξ_d	[m]	2			

2 shows the discrete scatterer contributions extracted from the measured time-variant PDPs in Fig. 1.

C. Radio Wave Propagation Model

As already mentioned in the introduction, the GSCM approach relies on very simplified ray-tracing methods. In this paper, the following assumptions were indeed made, namely

- Tx and Rx vehicles are driven at constant speeds v_{Tx} and v_{Rx} along a straight route in the same (or opposite) direction in a two-dimensional environment, such that the relative orientation of the Tx and Rx antenna patterns remains constant over time,
- The discrete mobile scatterers are moving at constant speeds v_p parallel to the Tx and Rx vehicles, without further traffic modeling,
- Only single-bounced reflections are considered, since they have been found to be the most significant propagation mechanism in V2V channels [17], [20].

The time-variant propagation delay τ_p (or, equivalently, the propagation distance d_p) and Doppler shift ν_p of the discrete scatterer contributions can hence be determined by the simple geometry relationships

$$\begin{cases} \tau_p = \tau_{\text{Tx}\to p}(t) + \tau_{p\to\text{Rx}}(t) \\ \nu_p = \dfrac{1}{\lambda}\left[(v_{\text{Tx}} - v_p)\cos\Omega_{\text{Tx},p} + (v_{\text{Rx}} - v_p)\cos\Omega_{\text{Rx},p}\right], \end{cases} \tag{4}$$

where λ is the wavelength of the system. Similar relationships can also be derived for the LoS component.

The number of discrete static (resp. mobile) scatterers in the simulated environment is given by the density $\chi_{p,s}$ (resp. $\chi_{p,m}$). Hence, using the two-dimensional environment geometry in Fig. 3 which is similar to the one in [17], we can generate

- Static discrete scatterers on both roadsides (and on the highway median strip). Their *x*- and *y*-coordinates are drawn from continuous uniform and multivariate normal distributions respectively, i.e. $x_{p,d} \sim \mathcal{U}(x_{d,\min}, x_{d,\max})$ and $y_{p,d} \sim L^{-1}\sum_{l=1}^{L}\mathcal{N}(\mu_{d,l}, \xi_d)$,

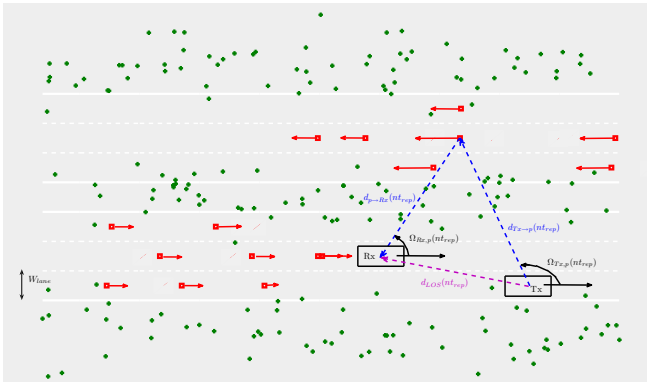

Fig. 3. Simplified two-dimensional geometry of the scattering environment for the modeling of the radio wave propagation in the highway environment. The green crosses (resp. red squares) correspond to discrete static (resp. mobile) scatterers.

- Mobile discrete scatterers on all the road lanes. As for static discrete scatterers, their initial *x*-coordinates are drawn from a continuous uniform distribution, whereas their *y*-coordinates are drawn from a discrete uniform distribution (with a number of outcomes equal to the total number of lanes N_{lanes}, each of width W_{lane}). They are also assigned a (realistic) constant speed along the *x*-axis, drawn from a truncated Gaussian distribution, so that too high (or negative, on a wrong lane) speeds are avoided.

The "birth/death" of the discrete scatterer contributions in the delay domain can be modeled by means of their maximum excess propagation distance (taken wrt. the LoS component) that was found to be best described by a lognormal distribution with mean $\mu_{b/d}$ and standard-deviation $\xi_{b/d}$, respectively. All the parameters for the modeling of the radio wave propagation aspects in each environment are given in Table II.

D. Discrete Scattering Model

The time-variant complex amplitude of the p^{th} discrete scatterer contribution is modeled as [17]

$$a_p \triangleq \underbrace{P_p^{1/2}}_{1)}\underbrace{g_p e^{j\phi_p}}_{2)}. \tag{5}$$

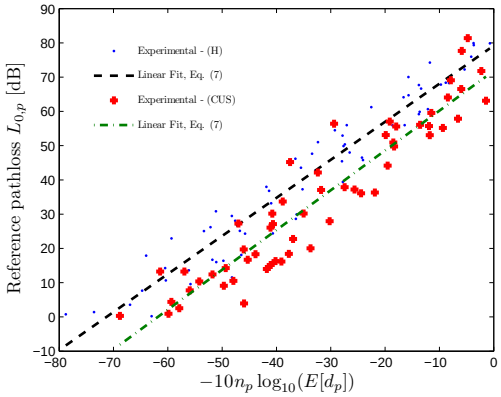

Fig. 4. Reference pathloss $L_{0,p}$ vs. propagation distance for the discrete scatterer contributions in the (H) and (CUS) environments.

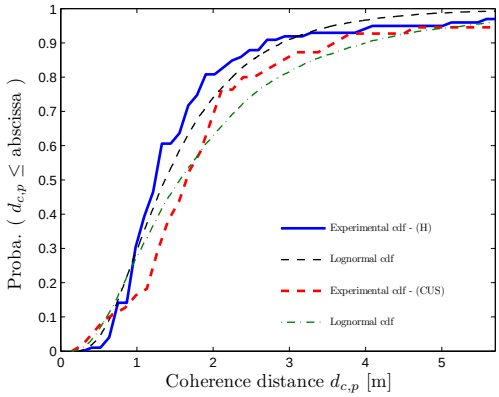

Fig. 5. CDFs of the large-scale fading standard-deviation $\sigma_{s,p,[\mathrm{dB}]}$ for the discrete scatterer contributions in the (H) and (CUS) environments.

The LoS component is modeled similarly, by only replacing the sub-index p by LoS. The two different processes in (5) correspond to, respectively

1) The time-variant average power of the discrete scatterer contribution: It is obtained by low-pass filtering the amplitude $|a_p(d_p)|^2$ with a 40λ sliding-average window [21], assuming Tx and Rx vehicles driven with an average speed $\bar{v} = 7.5$ km/h. The power of the low-pass filtered signal normalized wrt. the LoS one can be modeled such that (in the dB scale)

$$10\log_{10}\frac{P_p}{P_{\mathrm{LOS}}} = -\left[L_{0,p} + 10n_p\log_{10}(d_p) + S_p\right], \qquad (6)$$

where $L_p = L_{0,p} + 10n_p\log_{10}(d_p)$ and S_p correspond to the (distance-dependent) pathloss and the (stochastic) large-scale fading, respectively. Hence, a pathloss exponent $n_p > 0$ and the corresponding pathloss reference power $L_{0,p} > 0$ were extracted for each discrete scatterer contribution, as well as a number of S_p values.

Over all the extracted discrete scatterer contributions, the pathloss exponent n_p is found to be uniformly distributed, i.e. $n_p \sim \mathcal{U}(0, n_{\max})$, while $L_{0,p}$ can be modeled, as shown in Fig. 4, such that

$$L_{0,p} \sim 10\eta_{\Lambda_0}\log_{10}\left(E\left[d_p\right]^{-n_p}\right) + \Lambda_0, \qquad (7)$$

where Λ_0 is a Gaussian random variable with mean μ_{Λ_0} and standard-deviation ξ_{Λ_0}. For the LoS component, the exponent n_{LoS} is arbitrarily fixed to 1.8 as reported in [22], as the inter-vehicle distance remained almost constant for each measurement route (i.e. the Tx and Rx vehicles were driven at roughly the same constant speed during short time intervals).

On the other hand, over all the extracted LoS components and discrete scatterer contributions, the large-scale fading S_p can be modeled (in the dB scale) by a Gaussian random process, with autocorrelation function [17]

$$r_p(\Delta d) = \sigma_{S,p}^2 e^{-\log 2(\Delta d/d_{c,p})^2}, \qquad (8)$$

where $\sigma_{S,p}$ and $d_{c,p}$ denote the standard-deviation and the 0.5-coherence distance of the Gaussian process, respectively. As shown in Fig. 5, the coherence distance $d_{c,p}$ is lognormally distributed (with mean μ_c and standard-deviation ξ_c), while the standard-deviation $\sigma_{S,p}$ is log-correlated with $d_{c,p}$, i.e.

$$\log\sigma_{S,p} \sim \eta_S\log(d_{c,p}) + K_S, \qquad (9)$$

where K_S denotes a Gaussian random variable with mean $\mu_S = \log\sigma_{S,0}$ and standard-deviation ξ_S,

2) The small-scale fading $g_p e^{j\phi_p}$: It corresponds to the out filtered signal when using the 40λ sliding-average window. Its envelope g_p is a white process over time best modeled by the flexible Weibull distribution, whose shape parameter β_p measures the fading severity (i.e. $\beta_p = 2$ yields the Rayleigh distribution, while $\beta_p < 2$ denotes "worse than Rayleigh" fading). The phase ϕ_p is uniformly distributed from 0 to 2π.

The shape parameter β_p is found to be Gaussian distributed (with mean μ_β and standard-deviation ξ_β). As the average power of the small-scale fading was normalized to one, the scale parameter α_p of the Weibull distribution can be obtained with $\alpha_p = 1/\sqrt{\Gamma(1+2/\beta_p)}$.

Concerning the parameterization of the discrete scattering, it has to be noted that only contributions spanning over sufficiently large distances were used for the extraction of reliable distance-dependent pathloss parameters (the other ones being discarded). Using the same criterion as in [17], their relative distances have to be such that $(d_{p,\max} - d_{p,\min})/(d_{p,\max} + d_{p,\min}) \geq 0.1$. Discrete scatterer contributions with pathloss parameters that do not verify the conditions associated with (6) were discarded as they would introduce unrealistic propagation effects. The total number of "valid" discrete scatterer contributions extracted from the measured CIRs in each environment is given in Table III. Owing to their relative scarcity in some of the environments, only two aggregated environments will be considered in the following, i.e. the highway (H) environment and the campus / urban / sub-urban (CUS) areas.

TABLE III
NUMBER OF "VALID" EXTRACTED DISCRETE SCATTERER CONTRIBUTIONS (AND MEASUREMENT ROUTES) IN EACH ENVIRONMENT

Campus	Urban	Sub-urban	Highway
10 (4)	1 (3)	16 (6)	67 (5)

TABLE IV
PARAMETERS OF THE DISCRETE SCATTERING IN THE (H) AND (CUS) ENVIRONMENTS

		Parameters	Unit	(CUS)	(H)
Pathloss	Exponent n_p	$n_{\max}$	-	3.00	3.05
	Reference pathloss $L_{0,p}$	η_{Λ_0}	-	1.16	1.11
		μ_{Λ_0}	[dB]	71.83	79.20
		ξ_{Λ_0}	[dB]	7.37	5.76
	Exponent n_{LoS}	-	-	1.80	
	Reference pathloss $L_{0,\text{LoS}}$	-	[dB]	0	
Large-scale fading	Coherence distance $d_{c,p}$	μ_c	[m]	0.44	0.31
		ξ_c	[m]	0.74	0.58
	Standard-deviation $\sigma_{S,p}$	η_S	-	0.56	0.38
		$\sigma_{S,0}$	[dB]	2.32	2.32
		ξ_S	-	0.25	0.27
Small-scale fading	Weibull shape parameter β_p	μ_β	-	2.05	1.97
		ξ_β	-	0.20	0.20

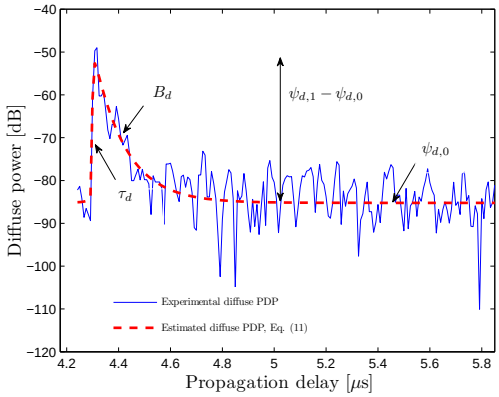

Fig. 6. Exemplary diffuse large-scale power and the corresponding least-square estimate in the (H) environment.

All parameters of the discrete scattering model in (H) and (CUS) environments are provided in Table IV.

E. Diffuse Scattering Model

Unlike [17] where the diffuse scattering was modeled by considering "walls" of roadside diffuse scatterers, a purely stochastic approach is chosen here, so that

$$h_d(\tau,t) \triangleq \underbrace{\psi_d^{1/2}(\tau,t)}_{1)}\underbrace{g_d(\tau)e^{j\phi_d}}_{2)}, \tag{10}$$

where the two different processes are, respectively

1) The large-scale power $\psi_d(\tau,t)$: It decays exponentially (in the dB scale) in the delay domain, as shown in Fig. 6, i.e.

$$\psi_{d,[\text{dB}]}(\tau,t) = \psi_{d,0} + \begin{cases} 0, & \tau < \tau_d \\ (\psi_{d,1}-\psi_{d,0})/2, & \tau = \tau_d \\ (\psi_{d,1}-\psi_{d,0})e^{-B_d(\tau-\tau_d)}, & \tau > \tau_d \end{cases}, \tag{11}$$

where $\psi_{d,1}$, $\psi_{d,0}$, B_d and τ_d are the maximum power, noise level, decay factor and base delay of the diffuse large-scale power, respectively. This model was first proposed in [18] for the description of the diffuse large-scale power in natural values, while it was modified in [23] to account for the sampled bandwidth-limited effects of the measurement system.

The parameters of the large-scale power were estimated with a non-linear least-square estimator, as described in [23]. The maximum power $\psi_{d,1}$ of the diffuse scattering is found to be correlated with the LoS distance, as reported in [23], [24] and as shown in Fig. 7, such that

$$\psi_{d,1} \sim \psi_{0,1} + 10\eta_{\Psi,1}\log_{10}(d_{\text{LOS}}) + \Psi_1, \tag{12}$$

where Ψ_1 denotes an exponentially correlated Gaussian random variable with zero-mean, standard-deviation $\xi_{\Psi,1}$ and 0.5-coherence distance $d_{\Psi,1}$, respectively. The noise level $\psi_{d,0}$ of the diffuse scattering is modeled similarly, by replacing the sub-index 1 by 0 in (12). The two Gaussian variables Ψ_0 and Ψ_1 are also correlated, with coefficient $\langle\Psi_0,\Psi_1\rangle$. The decay factor B_d is found to increase exponentially with the diffuse peak-to-noise ratio, such that

$$\log B_d \sim \log\left(e^{(\psi_{d,1}-\psi_{d,0})/\psi_B} - 1\right) + K_B, \tag{13}$$

where K_B is a Gaussian random variable with mean $\mu_B = \log B_0$ and standard-deviation ξ_B. Finally, the base-delay τ_d of the diffuse large-scale power is found to be highly correlated with the delay of the LoS component, such that

$$\tau_d = \tau_0 + \eta_\tau \tau_{\text{LOS}}, \tag{14}$$

2) The small-scale fading $g_d(\tau)e^{j\phi_d}$: Its envelope is found to be best described for each delay by the flexible Weibull distribution, with parameters $\beta_d(\tau)$ and $\alpha_d(\tau)$, while its phase ϕ_d is uniformly distributed between 0 and 2π.

As shown in Fig. 8, the shape parameter β_d can be described using the model given by (11), with a parameter set $\theta_\beta = [\beta_1\ \ \beta_0\ \ B_\beta\ \ \tau_\beta]$. Note that τ_β can also be defined wrt. the delay of the LoS component, i.e. $\tau_\beta = \tau_{\text{LOS}} + \Delta\tau_\beta$. A Gaussian

TABLE V
PARAMETERS OF THE DIFFUSE SCATTERING IN THE (H) AND (CUS) ENVIRONMENTS

		Parameters	Unit	(CUS)	(H)
Large-scale power	Maximum power $\psi_{d,1}$	$\psi_{0,1}$	[dB]	7.93	0.41
		$\eta_{\Psi,1}$	-	-2.03	-1.80
		$\xi_{\Psi,1}$	[dB]	11.07	11.29
		$d_{\Psi,1}$	[m]	6.93	5.73
	Noise level $\psi_{d,0}$	$\psi_{d,0}$	[dB]	-37.51	-29.49
		$\eta_{\Psi,0}$	-	-1.80	-2.07
		$\xi_{\Psi,0}$	[dB]	5.82	5.36
		$d_{\Psi,0}$	[m]	12.34	11.38
		$\langle \Psi_0, \Psi_1 \rangle$	-	0.56	0.43
	Decay factor B_d	ψ_B	[dB]	25.02	26.10
		B_0	[MHz]	14.94	15.12
		ξ_B	-	0.32	0.41
	Base delay τ_d	τ_0	[ns]	-28.64	-26.64
		η_τ	-	1.00	1.00
Small-scale fading	Weibull shape parameter β_d	β_1	-	1.10	1.04
		β_0	-	2.01	1.94
		B_β	[MHz]	1.34	1.30
		$\Delta\tau_\beta$	[ns]	-15.41	24.00
		ξ_β	-	0.26	0.26
	Weibull scale parameter α_d	μ_α	-	1.31	1.29
		ξ_α	-	0.26	0.24

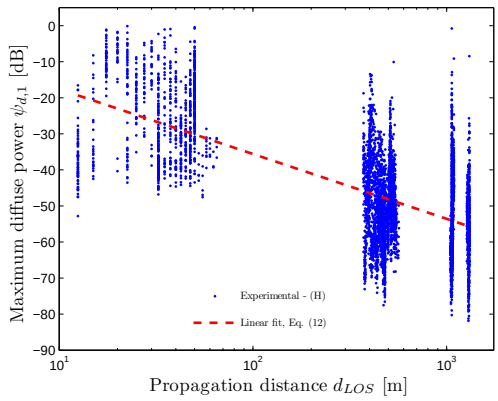

Fig. 7. Maximum power $\psi_{d,1}$ of the diffuse scattering vs. propagation distance in the (H) environment.

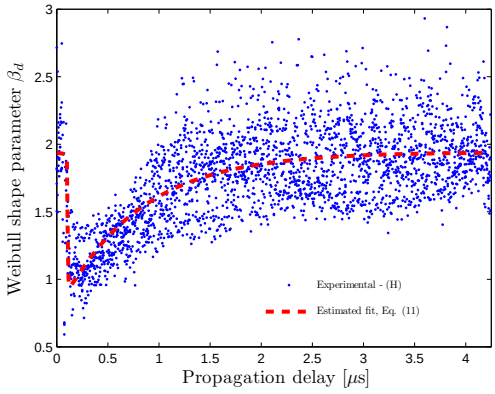

Fig. 8. Weibull shape parameter β_d of the diffuse small-scale fading vs. propagation delay in the (H) environment.

random variable with zero-mean and standard-deviation ξ_β was also accounted. As it can be observed, the severity of the diffuse small-scale fading can change from "worse than Rayleigh" (around the LoS component) to Rayleigh (as the delay increases, i.e. $\beta_d \to 2$ when $\tau \to \infty$). On the other hand, the scale parameter α_d is found to be Gaussian distributed, with mean μ_α and standard-deviation ξ_α.

Concerning the parameterization of the diffuse scattering, it has to be noted that it was done from the residual IRs (i.e. what remains after filtering out the detected LoS component and all the discrete scatterer contributions from the measured IRs), according to (2). Parameter sets $\theta_d = [\psi_{d,1} \;\; \psi_{d,0} \;\; B_d \;\; \tau_d]$ with a maximum power $\psi_{d,1}$ larger than the discrete peak power were discarded, as the detection of the discrete scatterer contributions would then not be possible. All parameters of the diffuse scattering model in (H) and (CUS) environments are provided in Table V.

IV. MODEL VALIDATION

We provide in this Section the procedure to simulate this V2V channel model as well as its validition, by comparing its performances with the ones obtained from the measured data.

A. Implementation Recipe

Realizations of this V2V wideband channel model can be generated with the following steps:

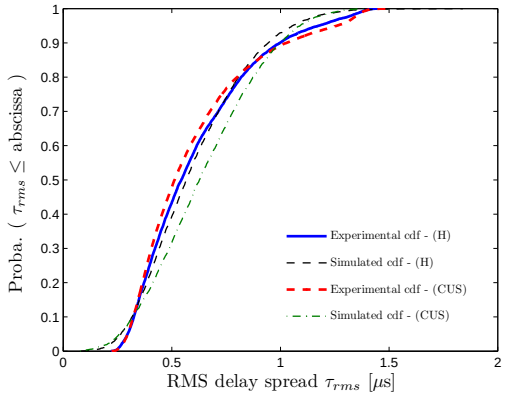

Fig. 9. RMS delay spread estimated from measured and simulated channel realizations in the (H) and (CUS) environments.

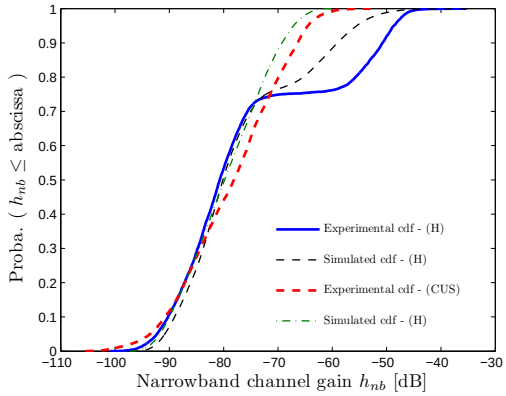

Fig. 10. Narrowband channel gain estimated from measured and simulated channel realizations in the (H) and (CUS) environments.

1) Determine the temporal (resp. delay) resolution t_{rep} (resp. $\Delta\tau$) as well as the total time duration and delay range of the simulation,
2) Specify the initial x- and y-coordinates of the Tx and Rx vehicles as well as their velocities v_{Tx} and v_{Rx}. Generate discrete static (resp. mobile) scatterers, with density $\chi_{p,s}$ (resp. $\chi_{p,m}$) and assign them (initial) *x*- and *y*-coordinates (as well as velocities for the mobile ones),
3) Estimate at each time instant the relative positions of the discrete scatterers wrt. the Tx and Rx vehicles in the simulated environment (assuming uniform linear motion along the *x*-axis only),
4) Estimate at each time instant the propagation distance d_p, the Angles of Departure (AoD) $\Omega_{\text{Tx},p}$ and Arrival (AoAs) $\Omega_{\text{Rx},p}$ for the LoS component and each single-bounced reflection on the discrete scatterers. Draw a value of the maximum excess propagation distance for each discrete scatterer contribution, in order to simulate their respective "birth/death" in the delay domain,
5) Draw pathloss, large- and small-scale fading statistics for the LoS component and each discrete scatterer contribution, given their respective propagation distance d_p (or d_{LOS}), as shown in Sec. III-D and with parameterization given in Table IV. Generate the corresponding time-variant complex amplitudes using (5),
6) Draw diffuse large-scale power (resp. diffuse small-scale fading) statistics at each time instant (resp. each delay tap), according to Sec. III-E and with parameterization given in Table V. Generate the corresponding time-variant complex diffuse scattering using (10),
7) Sum up at the Rx side the LoS component, the discrete scatterer contributions (including the bandlimited filter effects of the measurement system) and the diffuse scattering, according to (2).

B. Comparison with Measurements

The model validation is carried out by comparing metrics estimated from measured and simulated (through Monte-Carlo iterations) channel realizations in the (CUS) and (H) environments. Three different metrics were considered either in the delay- or time-domain, namely

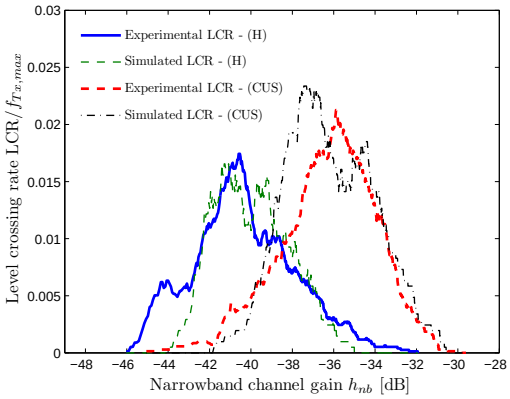

Fig. 11. Normalized LCR estimated from the equivalent narrowband envelope of exemplary measured and simulated channel realizations in the (H) and (CUS) environments.

1) Root-Mean-Square (RMS) delay spread: It characterizes at each time instant the dispersion of the power in the delay-domain. As shown in Fig. 9, there is a pretty good agreement between both the Cumulative Distribution Functions (CDFs) of the measured and simulated RMS delay spread. The Root-Mean Square Error (RMSE) between the measured and simulated CDFs is of 2.36% and 5.94% in the (H) and (CUS) environments, respectively. The simulated average RMS delay spreads of 58.90 and 63.99 μs are also found to be in good accordance with the measured ones of 60.88 and 59.82 μs in the (H) and (CUS) environments, respectively,

2) First-order statistics of the equivalent narrowband channel gain: The equivalent narrowband channel can be estimated from the time-variant IRs as

$$h_{\text{nb}}(t) = \frac{1}{K} \sum_{k=0}^{K-1} \left| h_{\text{Rx}}(\tau_k, t) \right| . \tag{15}$$

As shown in Fig. 10, there is a good agreement between the measured and simulated CDFs of the narrowband channel

gain in the (H) and (CUS) environments, with a RMSE of 4.77% and 3.23%, respectively. The measured and simulated distributions also match pretty well in terms of median, with a difference of 0.59 and 1.70 dB in the (H) and (CUS) environments, respectively. Finally, note that the gap between the measured and simulated CDFs in the (H) environment is due to one specific measurement route where the distance between the Tx and Rx vehicles was much smaller than for the other ones, hence resulting in a higher envelope level,

3) Level Crossing Rate (LCR): It characterizes the dynamics of the equivalent narrowband channel over time. The LCR is estimated from the large-scale variations of the narrowband channel. Indeed, the small-scale fading process of the discrete scatterer contributions can be undersampled as they can exhibit Doppler shifts larger than the maximum resolvable one $\nu_{\max}$ (limited to only 7.15 Hz). Hence, for a fair comparison, both the measured and simulated narrowband channels were low-pass filtered with a 40λ sliding-average window, in order to remove the small-scale fading. As shown in Fig. 11, the proposed channel model is found to be able to generate some specific simulated channel realizations with LCR very similar to the one that can be estimated for specific measurement routes in the (H) and (CUS) environments.

Hence, it is reasonable to assess the validity of the proposed V2V SISO channel model based on these three metrics, as they have not been directly used for its parameterization. Moreover, the comparison between the measured and simulated metrics shows that the model proposed in this paper is well suited for the modeling of V2V channels, despite the simplifying approximations that have been assumed (e.g. a simplified model for the scattering environment, only single-bounced reflections, etc.).

V. Conclusion

In this paper, we have presented a model for V2V radio propagation channels, based on an extensive measurement campaign conducted in different environments. The discrete scattering was described using a GSCM approach, which is particularly well-suited for modeling non-stationary (V2V) channels, as each discrete scatterer can be defined and characterized separately. Indeed, the radio wave propagation was modeled for each discrete scatterer contribution based on the assumption of single-bounced reflection processes, hence leading to a simplified geometry with lower complexity than ray-tracing methods. On the other hand, the scattering aspects were described stochastically using a classical fading model. Moreover, the diffuse scattering was investigated and included in the channel model, being characterized in a purely stochastic way. The complete parameterization was also provided, so that realizations of this V2V channel model can be easily generated. Moreover, it is interesting to note that, with a same framework for the GSCM approach (including the basic assumptions), the output of the proposed model stands well with the one developed in [17]. The validation of the simulated model shows good agreement with the measurement data, so that this model could be used for future validation of V2V communication systems.

Acknowledgment

This work was carried out in the framework of COST Action 2100 and EDA project n^o A-0935-RT-GC ICAR. The authors would like to thank Katsuyuki Haneda, Jukka Koivunen and Mikko Olkkonen for their participation in the measurement campaign, as well as the Belgian Fonds de la Recherche Scientifique and the SMARAD Centre of Excellence funding of the Academy of Finland for their financial support.

References

[1] 802.11p, "Draft amendment to wireless LAN medium access control (MAC) and physical layer (PHY) specifications: Wireless access in vehicular environments," *IEEE P802.11p/D0.26*, January 2006.

[2] A. F. Molisch, F. Tufvesson, J. Karedal, and C. F. Mecklenbräuker, "A survey on vehicle-to-vehicle propagation channels," *IEEE Wireless Communications*, vol. 16, no. 6, pp. 12 – 22, December 2009.

[3] C. X. Wang, X. Cheng, and D. I. Laurenson, "Vehicle-to-vehicle channel modeling and measurements: Recent advances and future challenges," *IEEE Communications Magazine*, vol. 4, no. 11, pp. 76 – 84, November 2009.

[4] J. Maurer, T. Fügen, and W. Wiesbeck, "Narrow-band measurement and analysis of the inter-vehicle transmission channel at 5.2 GHz," in *IEEE 55th Vehicular Technology Conference (VTC)*, vol. 3, Birmingham, Alabama, (USA), 2002, pp. 1274 – 1278.

[5] J. Maurer, T. Fügen, T. Schafer, and W. Wiesbeck, "A new inter-vehicle communications (IVC) channel model," in *IEEE 60th Vehicular Technology Conference (VTC)*, vol. 1, Los Angeles, California, (USA), September 2004, pp. 9 – 13.

[6] L. Reichardt, T. Fügen, and T. Zwick, "Influence of antenna placement on car to car communication channel," in *9th European Conference on Antennas and Propagation EuCAP*, Berlin (Germany), March 2009.

[7] G. Acosta and M. A. Ingram, "Model development for the wideband expressway vehicle-to-vehicle 2.4 GHz channel," in *IEEE Wireless Communications and Networking Conference (WCNC)*, vol. 3, Las Vegas, Nevada (USA), April 2006, pp. 1283 – 1288.

[8] G. Acosta-Marum and M. A. Ingram, "A BER-based partitioned model for a 2.4 GHz vehicle-to-vehicle expressway channel," *Wireless Personal Communications*, vol. 37, pp. 421 – 443, May 2006.

[9] O. Renaudin, V. M. Kolmonen, P. Vainikainen, and C. Oestges, "Non-stationary narrowband MIMO inter-vehicle channel characterization in the 5 GHz band," *IEEE Transactions on Vehicular Technology*, vol. 59, no. 4, pp. 2007 – 2015, May 2010.

[10] L. Bernadó, T. Zemen, J. Karedal, A. Paier, A. Thiel, O. Klemp, N. Czink, F. Tufvesson, A. F. Molisch, and C. F. Mecklenbräuker, "Time-, frequency-, and space-varying K-factor analysis of V2V street crossing radio channels," in *IEEE International Symposium on Personal, Indoor and Mobile Radio Communications (PIMRC)*, September 2010.

[11] D. W. Matolak, I. Sen, and W. Xiong, "The 5 GHz airport surface area channel - Part I: Measurement and modeling results for large airports," *IEEE Transactions on Vehicular Technology*, vol. 57, no. 4, pp. 2014 – 2026, July 2008.

[12] O. Renaudin, V. M. Kolmonen, P. Vainikainen, and C. Oestges, "Car-to-car channel models based on wideband MIMO measurements at 5.3 GHz," in *9th European Conference on Antennas and Propagation (EUCAP)*, Berlin (Germany), March 2009.

[13] M. Pätzold, B. Hogstad, and N. Youssef, "Modeling, analysis, and simulation of MIMO mobile-to-mobile fading channels," *IEEE Transactions on Wireless Communications*, vol. 7, no. 2, pp. 510 – 520, February 2008.

[14] A. G. Zajić, G. L. Stüber, T. G. Pratt, and S. T. Nguyen, "Wideband MIMO mobile-to-mobile channels: Geometry-based statistical modeling with experimental validation," *IEEE Transactions on Vehicular Technology*, vol. 58, no. 2, pp. 517 – 534, February 2009.

[15] X. Cheng, C. X. Wang, D. I. Laurenson, S. Salous, and A. V. Vasilakos, "An adaptive geometry-based stochastic model for non-isotropic MIMO mobile-to-mobile channel," *IEEE Transactions on Wireless Communications*, vol. 8, no. 9, pp. 4824 – 4835, September 2009.

[16] A. F. Molisch, "A generic channel model for MIMO wireless propagation channels in macro- and microcells," *IEEE Transactions on Signal Processing*, vol. 52, no. 1, pp. 61 – 71, January 2004.

[17] J. Karedal, F. Tufvesson, N. Czink, A. Paier, C. Dumard, T. Zemen, C. F. Mecklenbräuker, and A. F. Molisch, "A geometry-based stochastic MIMO model for vehicle-to-vehicle communications," *IEEE Transactions on Wireless Communications*, vol. 8, no. 7, pp. 3646 – 3657, July 2009.
[18] A. Richter, "Estimation of radio channel parameters: Models and algorithms," Ph.D. dissertation, Technischen Universität Ilmenau, 2005.
[19] V. M. Kolmonen, J. Kivinen, L. Vuokko, and P. Vainikainen, "5.3-GHz MIMO radio channel sounder," *IEEE Transactions on Instrumentation and Measurement*, vol. 55, no. 4, pp. 1263–1269, August 2006.
[20] T. Abbas, J. Karedal, F. Tufvesson, A. Paier, L. Bernadó, and A. F. Molisch, "Directional analysis of vehicle-to-vehicle propagation in different traffic environments," in *IEEE 73rd Vehicular Technology Conference (VTC)*, Budapest (Hungary), May 2011, pp. 1 – 5.
[21] W. C. Y. Lee, "Estimate of local average power of a mobile radio channel," *IEEE Transactions on Vehicular Technology*, vol. 34, no. 1, pp. 22– 27, February 1985.
[22] A. Paier, J. Karedal, N. Czink, H. Hofstetter, C. Dumard, T. Zemen, F. Tufvesson, A. F. Molisch, and C. F. Mecklenbräuker, "Car-to-car radio channel measurements at 5 GHz: Pathloss, power-delay profile and delay-Doppler spectrum," in *IEEE International Symposium on Wireless Communication Systems (ISWCS)*, Trondheim, (Norway), October 2007, pp. 224 – 228.
[23] N. Czink, A. Richter, E. Bonek, J. P. Nuutinen, and J. Ylitalo, "Including diffuse multipath parameters in MIMO channel models," in *IEEE 66th Vehicular Technology Conference (VTC)*, September 2007, pp. 874 – 878.
[24] T. Santos, J. Karedal, P. Almers, F. Tufvesson, and A. F. Molisch, "Modeling the ultra-wideband outdoor channel: Measurements and parameter extraction method," *IEEE Transactions on Wireless Communications*, vol. 9, no. 1, pp. 282 – 290, January 2010.

Olivier Renaudin received in 2006 the diploma of engineer in telecommunications from the Ecole Nationale Supérieure d'Electronique, Informatique et Radiocommunications de Bordeaux and the M.Sc. degree in signal processing from the University of Bordeaux I, France. In February 2007, he joined the Microwave Laboratory at the Université catholique de Louvain (UCL), where is currently working on his doctoral thesis. His research interests are channel sounding and channel modeling for vehicular communication networks.

Veli-Matti Kolmonen received the M.Sc. degree in technology from Helsinki University of Technology (TKK), Espoo, Finland, in 2004 and the D.Sc. degree in technology from Aalto University, Espoo, Finland in 2010. During 2003-2012, he was with the Department of Radio Science and Engineering, TKK (Aalto University as of 2010), first as a Research Assistant, Researcher, and Post-Doctoral Researcher. Currently his is with Philips Medical Systems MR Finland.

Pertti Vainikainen received the degree of Master of Science in Technology, Licentiate of Science in Technology and Doctor of Science in Technology from Helsinki University of Technology (TKK) in 1982, 1989 and 1991, respectively. From 1992 to 1993 he was Acting Professor of Radio Engineering, since 1993 Associate Professor of Radio Engineering and since 1998 Professor in Radio Engineering, all in the Radio Laboratory (since 2008 Department of Radio Science and Engineering)of TKK (since 2010 Aalto University). In 1993-97 he was the director of the Institute of Radio Communications (IRC) of TKK, and a visiting professor in 2000 at Aalborg University, Denmark and in 2006 at University of Nice in France. His main fields of interest are antennas and propagation in radio communications and industrial measurement applications of radio waves. He is the author or co-author of 6 books or book chapters and about 320 refereed international journal or conference publications and the holder of 11 patents.

Claude Oestges received the M.Sc. and Ph.D. degrees in Electrical Engineering from the Universit catholique de Louvain (UCLouvain), Louvain-la-Neuve, Belgium, respectively in 1996 and 2000. In January 2001, he joined as a post-doctoral scholar the Smart Antennas Research Group (Information Systems Laboratory), Stanford University, CA, USA. From January 2002 to September 2005, he was associated with the Microwave Laboratory UCLouvain as a post-doctoral fellow of the Belgian Fonds de la Recherche Scientifique (FRS-FNRS). Claude Oestges is presently a FRS Research Associate and Associate Professor with the Electrical Engineering Department, Institute for Information and Communication Technologies, Electronics and Applied Mathematics (ICTEAM), UCLouvain.